Journal of Power Sources 220 (2012) 331–341

Contents lists available at SciVerse ScienceDirect

Journal of Power Sources

journal homepage: www.elsevier.com/locate/jpowsour

The analyses of the start-up process of a planar, anode-supported solid oxide fuel cell using three different start-up procedures

Ming-Hong Chen [a], Tsung Leo Jiang [b,*]

[a] Environmental and Energy Technology Center, Institute of Nuclear Energy Research, Atomic Energy Council, Taoyuan 32546, Taiwan, ROC
[b] Department of Aeronautics and Astronautics, National Cheng Kung University, No.1, University Road, Tainan 70101, Taiwan, ROC

HIGHLIGHTS

- Three start-up procedures for an anode-supported planar SOFC are investigated.
- The largest absolute temperature-gradient is exhibited in the early stage.
- The anode-recycling start-up procedure significantly reduces the start-up time.
- The fixed-temperature-difference procedure may reduce the temperature-gradient.
- The fixed-temperature-difference procedure also reduces the start-up time.

ARTICLE INFO

Article history:
Received 17 April 2012
Received in revised form
4 August 2012
Accepted 6 August 2012
Available online 11 August 2012

Keywords:
Solid oxide fuel cell
Transient
Simulation
Start-up

ABSTRACT

Three start-up procedures for an anode-supported planar SOFC are proposed and investigated numerically in the present study. The first is to introduce the inlet fuel at the operation temperature after the heat-up process is completed. The second is to incorporate the anode-recycling mechanism into the start-up process. The third is to fix the difference between the inlet-fuel temperature and the cell minimum temperature. The numerical results obtained from the present study show that the effective maximum absolute temperature-gradient is exhibited in the early stage of the start-up process. For the present investigated SOFC configuration, the required start-up time for the case using methane is 3.2-fold longer than that using hydrogen. The effective maximum absolute temperature-gradient for the case using hydrogen is 2.2-fold larger than that utilizing methane. The endothermic internal reforming reaction of methane has a positive effect on the accommodation of the temperature uniformity during the start-up process. The anode-recycling mechanism significantly reduces the start-up time For the fixed-temperature-difference start-up procedure, a properly selected temperature difference may lead to a smaller effective maximum absolute temperature-gradient in the early stage and a shorter start-up time by accelerating the start-up pace in the later stage.

1. Introduction

The solid oxide fuel cell (SOFC), which directly converts the chemical energy into electrical power via the electrochemical reaction, is one of the most attractive candidates for the next generation of power sources [1]. Among the several kinds of geometry design, the planar SOFC has higher energy conversion efficiency and a lower manufacturing cost than the tubular SOFC [2,3]. In order to reduce the resistance of the ionic conduction, an extremely thin electrolyte (e.g. 8 μm) is usually employed in the positive electrode, electrolyte and negative electrode (PEN) structure. However, the thermal shock during the transient operations, such as the heat-up, the start-up, the load change and the cool-down processes, may damage the structure robustness of the ultra-thin electrolyte and the durability of the cell, since the cell temperature varies in a broad range from 25 to 800 °C.

Due to the high operating temperature (700 – 1000 °C), the SOFC has to undergo the heat-up and start-up processes to warm-up the cell from the room temperature (25 °C) to the operable level (around 800 °C). If the cell temperature rises too fast, it will lead to a serious internal temperature-gradient increase and significant differences of the thermal-expansion rates of the cell components, resulting in a high thermal stress [4] and reducing the cell performance and its durability. As this is especially true for the planar

* Corresponding author. Tel.: +886 6 2757575x63676; fax: +886 6 2389940.
E-mail address: jiang@mail.ncku.edu.tw (T.L. Jiang).

0378-7753/$ – see front matter © 2012 Elsevier B.V. All rights reserved.
http://dx.doi.org/10.1016/j.jpowsour.2012.08.018

Nomenclature

C_2	Inertial resistance factor (m^{-1})
C_p	Specific heat (J kg^{-1} K^{-1})
D_i	Diffusivity for the *i*th species (m^2 s^{-1})
D_p	Particle diameter in porous zone (μm)
D_{eff}	Effective diffusivity (m^2 s^{-1})
E	Total energy (J)
E_0	Theoretical potential (V)
E_a	Activation energy (kJ mol^{-1})
E_{anode}	Activation energy for exchange current density of anode (kJ mol^{-1})
$E_{cathode}$	Activation energy for exchange current density of cathode (kJ mol^{-1})
E_f	Total energy of fluid (J)
E_{OCV}	Open circuit voltage (V)
F	Faraday constant (C mol^{-1})
G^0	Gibbs free energy for the electrochemical reaction (J mol^{-1})
H_{Ox}	Enthalpy of oxidation (J mol^{-1})
h_i	Species enthalpy (J mol^{-1})
h_j^0	Standard state enthalpy (J mol^{-1})
i	Current density (A cm^{-2})
i_0	Exchange current density (A cm^{-2})
J_i	Mass diffusion flux for *i*th species (kg m^{-2} s^{-1})
k	Rate constant (mol m^{-2} bar^{-1} s^{-1})
k_0	Pre-exponential factor (mol m^{-2} bar^{-1} s^{-1})
k_a	Pre-exponential factor for exchange current density of anode (A cm^{-2})
k_c	Pre-exponential factor for exchange current density of cathode (A cm^{-2})
k_{eff}	Effective thermal conductivity (W m^{-1} K^{-1})
k_f	Fluid thermal conductivity (W m^{-1} K^{-1})
k_s	Solid thermal conductivity (W m^{-1} K^{-1})
K_{WGS}	Equilibrium constant for water gas shift reaction
L	Cell length (mm)
$\dot{m}$	Mass flow rate (kg s^{-1})
M_i	Molecular weight (g mol^{-1})
n	Number of electron transfer
N	Number of species (−)
P	Pressure (atm)
p_{atm}	Atmospheric pressure (atm)
p_i^{tpb}	Partial pressure for the *i*th species near the triple phase boundary (atm)
Q	Thermal energy (J)
R_i	Chemical reaction rate (mol m^{-3} s^{-1})
R_{ohm}	Ohmic resistance (Ω cm^{-2})
R	Gas constant (J mol^{-1} K^{-1})
S_i^h	Fluid enthalpy source term (J m^{-3} s^{-1})
$\frac{\partial(\varepsilon\rho\vec{v})}{\partial t}+\nabla\cdot(\varepsilon\rho\vec{v}\vec{v})=-\varepsilon\nabla p+\nabla\cdot(\varepsilon\bar{\bar{\tau}})+S_M$	Standard state entropy (J mol^{-1} K^{-1})
S_M	Momentum-sink term in porous (N m^{-3})
T	Temperature (K)
x	X coordinate (mm)
X	x/L, dimensionless coordinate along the cell length (−)
V_{cell}	Cell voltage (V)
Y_i	Mass fraction for the *i*th species

Greek letters

α	Permeability (m^2)
β	Transfer coefficient
γ	The extent of the anode-recycling
ε	Porosity
η_{act}	Activation overpotential (V)
η_{conc}	Concentration overpotential (V)
μ	Dynamic viscosity (Pa s)
ν_j'	Stoichiometric coefficient for *j* reactant
ν_j''	Stoichiometric coefficient for *j* product
ρ	Density (kg m^{-3})
$\bar{\bar{\tau}}$	Stress tensor (−)
υ	Velocity (m s^{-1})

Abbreviation

APU	Auxiliary power unit
DISR	Direct internal steam reforming
EC	Electrochemical
LSM	Lanthanum strontium manganite
PEN	Positive-electrolyte-negative
TPB	Triple-phase-boundary
WGS	Water gas shift reaction
YSZ	Yttria-stablized zirconia

SOFC, the management of the temperature uniformity of the planar SOFC deserves in-depth investigations.

The start-up process is usually initiated by feeding the fuel into the fuel channel after the SOFC is heated up to around 600 °C by a proper heating strategy as investigated in our previous work [5]. There are two kinds of fuel reported to be employed in the start-up process, i.e., hydrogen and hydrocarbon [6–10]. For instance, Selimovic et al. [9] investigated the start-up time and the maximum temperature gradient by feeding hydrogen and methane as the fuel, respectively, for the start-up process of a planar SOFC. It was found that the required time for the case using methane (1 h) is 2-fold longer than that using hydrogen (30 min). For the case using hydrogen, the maximum temperature gradient occurs at the beginning of the start-up process, with the value about 5 K cm^{-1}, and drastically drops thereafter. For the case using methane, the temperature gradient keeps increasing during the whole start-up process, and reaches the maximum value, about 11 K cm^{-1} at the end of the start-up process. Petruzzi et al. [8] showed that the temperature of 600 °C is the most appropriate state to proceed the start-up process. In their 3.5 kW auxiliary power unit (APU) system, the start-up process takes about 35 min, which is too slow for their APU system. Lin and Hong [11] built a 250 kW turbo-SOFC-system model to investigate the start-up process. As the fuel inlet pressure is 2 atm, the start-up process takes about 1.3 h. They also showed that the most important factor affecting the start-up time is the response of the stack temperature of the SOFC system. They also suggested a practically applicable method to accelerate the start-up process, i.e., increasing the inlet pressure. As the inlet pressure increases from 2 atm to 3 atm, the start-up time is shortened to 1 h. However, the temperature-gradient variations are not investigated in their study. Lin and Hong [12] investigated the cold start-up process of a 100 W SOFC-APU system by their in-house developed numerical model. In their system, the embedded burner and the recycling mechanism were incorporated in their model. By neglecting the effect of the temperature gradient, it takes 100 s for the SOFC-APU system to reach the steady state. However, they also mentioned that such a fast start-up pace will lead to the problems of the significant temperature gradient, thermal stress, and fatal component fracture. Therefore, a nonlinear sliding-observer was developed in their model to obtain the instantaneous variation of

the cell temperature. They also mentioned that such an observer is a useful tool for the development of a quick start-up system. By feeding back the instantaneous cell temperature to the control unit, the high temperature gradient can be avoided in the start-up process. Wang et al. [10] concluded that the dynamic response and the structure integrity are significant issues for the quick start-up process of the SOFC-APU system. Cheekatamarla et al. [7] experimented with the start-up process of a SOFC system by feeding hydrogen into the cell at first. As the cell temperature reached to the normal operation level (~800 °C), the fuel was switched to propane. Barzi et al. [6] used hydrogen as the fuel to investigate the start-up process of a tubular SOFC. With the condition of 70% of the fuel utilization rate and 800 °C as the inlet temperature, the start-up process takes about 3 h. However, the corresponding temperature gradient within the cell was not evaluated. In order to reduce the temperature gradient in the cell, Nikooyeh et al. [13] incorporated the anode-recycling mechanism in the steady-state analysis of the SOFC system. It was found that the temperature gradient reduces about 38% as the anode-recycling level is 75%. However, the effect of anode-recycling mechanism on the start-up process was not conducted.

For the above reviewed studies about the start-up process, it was found that the start-up pace is generally too slow, especially for the APU system. As the most studies were focused on the start-up time, the variation of the temperature gradient in the SOFC was not comprehensively evaluated to a satisfactory level. A complete evaluation for the performance of the start-up process should take into account not only the start-up time but also the detailed distribution of the temperature gradient.

In the present study, a finite-volume model is developed to investigate the temperature variation, the start-up time and the corresponding temperature gradient for an anode-supported planar SOFC during the start-up process. A comprehensive numerical simulation model, employing the finite-volume approach, has been developed for the three-dimensional, multi-component, electrochemically, and chemically reacting flow of a single planar SOFC unit cell. Three start-up procedures are proposed and investigated. The first is to introduce the inlet fuel at the operation temperature of 800 °C after the heat-up process is completed. The second is to incorporate the anode-recycling mechanism into the start-up process. The third is to fix the difference between the inlet-fuel temperature and the cell minimum temperature. The effect of the fuel type employed on the start-up process is also evaluated.

2. Model and formulation

2.1. Start-up approach

For the start-up process, the steam/carbon ratio and mass flow rate are selected to keep the start-up time within 1 h. To initiate the start-up process, the fuel stream is fed into the fuel channel and air is fed into the air channel. For the thermal condition, the inlet temperature is switched from the state of the end of heat-up process to 1073 K at the beginning of the start-up process [6]. Two kinds of fuel, i.e., hydrogen and methane are employed for the start-up process. For the case using hydrogen, only the electrochemical reaction occurs within the SOFC. For the case using methane, the direct internal steam reforming (DISR), water gas shift (WGS) and the electrochemical reaction are considered in the start-up process. The initial temperature distribution is adopted from the optimal heat-up results of our previous study [5]. The start-up process finishes as the average cell temperature reaches to 99% of the steady-state value.

2.2. Anode supported planar SOFC

A finite-volume, three-dimensional numerical model for an anode-supported planar SOFC cell unit is developed using the commercial software FLUENT with the Gambit as the preprocessor [14]. The grid system of the multi-zones for the anode channel, the cathode channel, the interconnector and the PEN structure, is constructed by the Gambit. The conservation equations of mass, species, momentum and energy with proper designated boundary conditions are solved by the FLUENT.

The geometry of the investigated planar SOFC is shown in Fig. 1a and the component specification is shown in Fig. 1b. There are 20 unit cells on each single cell plate, and 10 repeated single cell plate for the whole SOFC stack. With the power density of 0.62 W cm^{-2}, the power of the SOFC stack is about 620 W. Due to the planar geometry, it is commonly assumed that each unit cell has the same properties, i.e., species and temperature distributions. It is assumed that the stack is well insulated [8] during the transient operations, and the heat loss of the unit cell at the edge is negligible. Due to the symmetric boundary conditions for each cell, all the cells will thus behave in the same way approximately. A quantitative verification [13] also showed that the temperature variation is within 1 K for over 90% cells. Therefore, one can compute only one unit cell and extend the results to the whole plate of the cell, as shown in Fig. 1a. The geometry data of the planar SOFC is shown in Table 1. With the symmetric feature of the planar SOFC, only a half of the unit cell is built in the finite-volume model. In the following results, the dimension is normalized from 0 to 1. The detail parameters for the SOFC system specification are listed in Table 1.

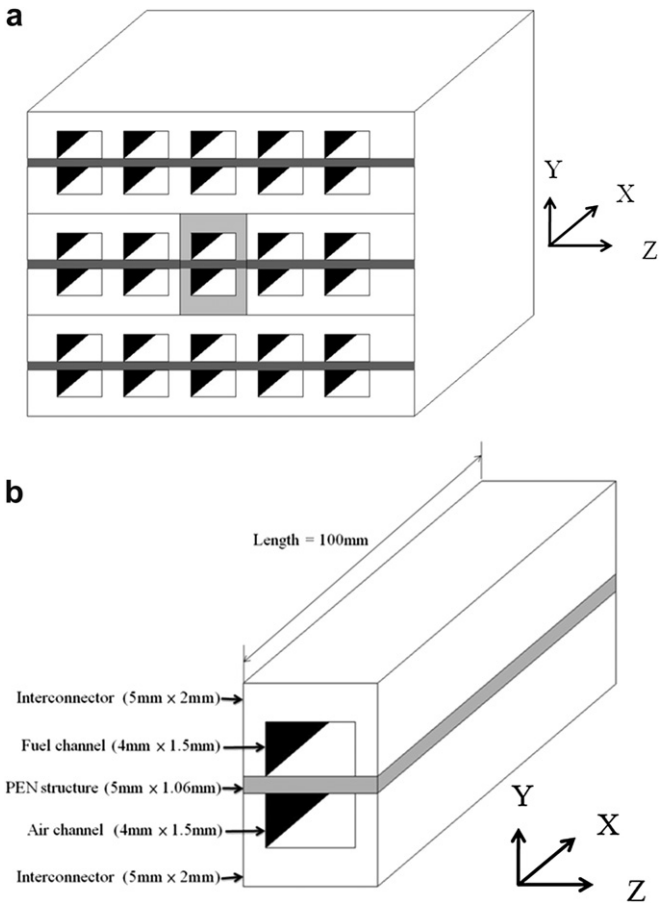

Fig. 1. Schematic diagram of the anode-supported planar SOFC for (a) stack, (b) unit cell and component specifications.

Table 1
The SOFC system specifications.

Anode thickness	1000 μm
Electrolyte thickness	10 μm
Cathode thickness	50 μm
Cell dimension	10 cm × 10 cm
Outer channel dimension	5 mm × 2 mm
Inner channel dimension	4 mm × 1.5 mm
Air to fuel ratio	8
Steam to carbon ratio	2
Fuel utilization rate	70%
Inlet temperature	1073 K
Operating Pressure	1 atm

2.3. Conservation equations

The conservation equations for the start-up operation are described in terms of the porosity. For the non-porous regions, the porosity is equal to unity. The porosities for various materials are listed in Table 2. The mass conservation equation for the finite volume model is:

$$\frac{\partial(\varepsilon\rho)}{\partial t} + \nabla\cdot(\varepsilon\rho\vec{v}) = 0 \tag{1}$$

The momentum conservation equation is:

$$\frac{\partial(\varepsilon\rho\vec{v})}{\partial t} + \nabla\cdot(\varepsilon\rho\vec{v}\vec{v}) = -\varepsilon\nabla p + \nabla\cdot(\varepsilon\bar{\bar{\tau}}) + S_M \tag{2}$$

where $\bar{\bar{\tau}}$ is stress tensor, and S_M is the momentum sink term for the porous media. The latter is evaluated by:

$$S_M = -\left(\frac{\mu}{\alpha}v_i + C_2\frac{1}{2}\rho v_{mag}v_i\right) \tag{3}$$

The inertial resistance C_2 is evaluated by:

$$C_2 = \frac{3.5}{D_p}\frac{(1-\varepsilon)}{\varepsilon^3} \tag{4}$$

where D_p is the average particle diameter, and ε is the porosity. Those parameters are listed in Table 2.

For the species conservation equation, the source/sink term for the chemical and electrochemical reactions are considered [15]:

$$\frac{\partial(\varepsilon\rho Y_i)}{\partial t} + \nabla\cdot(\varepsilon\rho\vec{v}Y_i) = \nabla\cdot(\varepsilon\rho D_i\nabla Y_i) + \sum_{i=1}^{N} M_i R_i + S_i \tag{5}$$

Table 2
Physical properties.

Property	Anode (Ni-doped YSZ)	Cathode (LSM)	Electrolyte (YSZ)	Interconnector (Stainless steel)
Density (kg m^{-3})	3030 [34]	3310 [34]	5163 [34]	8030 [34]
Conductivity (W m^{-1} K^{-1})	5.84 [34]	1.86 [34]	2.16 [34]	20.0 [34]
Specific heat (J kg^{-1} K^{-1})	595 [34]	573 [34]	606 [34]	502 [34]
Permeability (−)	3.4×10^{-2} [35]	3.7×10^{-2} [35]	1.0×10^{-18} [31]	1.0×10^{-18} [31]
Porosity (−)	0.42 [35]	0.36 [35]	1.0×10^{-5} [31]	1.0×10^{-5} [31]
Average particle diameter (μm)	1.40[a]	1.40[a]	1.0[a]	1.0[a]

[a] Assumed value.

where R_i is the species production by chemical reactions, i.e., DISR and WGS, as described above, and S_i is the sink/source due to H_2 electrochemical reaction. The latter can be expressed according to the Faraday's law as:

$$\text{Anode}: \quad S_{H_2} = \frac{-i}{nF} \tag{6}$$

$$S_{H_2O} = \frac{i}{nF} \tag{7}$$

$$\text{Cathode}: \quad S_{O_2} = \frac{-i}{nF} \tag{8}$$

where n is the number of electrons transferred in the electrochemical reaction with 2 for the anode and 4 for the cathode. The energy conservation equation also takes the chemical and electrochemical reactions into account, and is given as [15]:

$$\frac{\partial(\varepsilon\rho E)}{\partial t} + \nabla\cdot[\vec{v}(\varepsilon\rho E + \varepsilon p)] = \nabla\cdot\left[\varepsilon k_{eff}\nabla T - \left(\sum_i \varepsilon h_i J_i\right) + (\varepsilon\bar{\bar{\tau}}\cdot\vec{v})\right] - \sum_i^N \varepsilon h_i^0 R_i + S_f^h \tag{9}$$

where S_f^h is the fluid enthalpy source term which will be described below. The effective conductivity in the porous media is evaluated from the fluid conductivity, the solid conductivity, and the porosity as [16]:

$$k_{eff} = \varepsilon k_f + (1-\varepsilon)k_s \tag{10}$$

In the energy equation, the energy source terms due to the ohmic heating corresponding to the electrochemical reaction can be expressed as:

$$S_{energy\_ohm} = i^2 R_{ohm} \tag{11}$$

Another energy source term in Eq. (9) is due to the electrochemical reaction and can be expressed as [13]:

$$S_{energy\_electrochemical} = i\left(\frac{\Delta H_{Ox}}{nF} - V_{cell}\right) \tag{12}$$

where ΔH_{Ox} is the enthalpy of oxidation. Since the inner temperature gradient is modest, the interior radiation is negligible [17]. On the outer surface, a properly designed insulation case is supposed to keep the stack wall temperature below 400 K [8]. Furthermore, the quantitative evaluation showed that the radiation was minor in the SOFC, specifically, only about 0.6% [18]. Therefore, the thermal radiation is not considered in the present model.

2.4. Chemical reactions

In the fuel side, the fast and endothermic DISR reaction (Eq. (13)) converts CH_4 to H_2 for the electrochemical reaction and CO for the subsequent WGS reaction. The latter reaction is to generate more H_2 and some CO_2 (Eq. (14)).

$$CH_4 + H_2O \leftrightarrow 3H_2 + CO \tag{13}$$

$$CO + H_2O \leftrightarrow H_2 + CO_2 \tag{14}$$

The DISR reaction includes many intermediate radicals and complicated intermediate reactions, such as absorption, desorption and decomposition. In the present study, the DISR reaction is

reduced to a two-equation mode, since it has been proven to be able to provide adequate predictions for the simulation of the SOFC [11,13,19–21]. The rate constants for the above reactions are described by the Arrhenius expression:

$$k = k_0 e^{-E_a/RT} \tag{15}$$

Although the WGS is usually assumed to be equilibrium [22], a simple kinetic model including forward and backward reactions is employed in the present model in order to account for the dynamic change of the species in the start-up process. The related parameters for the chemical reactions of the DISR and WGS reactions applied in the present FV model are [23,24]:

$$k_{0,\mathrm{IR}} = 4274\ \mathrm{mol\ m^{-2}\ bar^{-1}\ s^{-1}} \tag{16a}$$

$$E_{a,\mathrm{IR}} = 82\ \mathrm{kJ\ mol^{-1}} \tag{16b}$$

$$k_{0,\mathrm{WGS,forward}} = 0.0171\ \mathrm{mol\ m^{-3}\ Pa^{-2}\ s^{-1}} \tag{17a}$$

$$E_{a,\mathrm{WGS}} = 103\ \mathrm{kJ\ mol^{-1}} \tag{17b}$$

The backward reaction rate of WGS is derived from the equilibrium constant as:

$$k_{0,\mathrm{WGS,backward}} = \frac{k_{0,\mathrm{WGS,forward}}}{K_{\mathrm{WGS}}} \tag{18}$$

The equilibrium constant is evaluated by:

$$K_{\mathrm{WGS}} = \exp\left(\frac{\Delta S^0_{\mathrm{WGS}}}{R} - \frac{\Delta H^0_{\mathrm{WGS}}}{RT}\right)\left(\frac{p_{\mathrm{atm}}}{RT}\right)^{\left(\nu''_j - \nu'_j\right)}, \tag{19}$$

where ν''_j is the stoichiometric coefficient of the product and ν'_j is that of the reactant. The term p_{atm} denotes the atmospheric pressure. The term within the exponential function represents the change in Gibbs free energy, and can be computed as follows:

$$\frac{\Delta S^0_{\mathrm{WGS}}}{R} = \sum_{j=1}^{N}\left(\nu''_j - \nu'_j\right)\frac{S^0_j}{R} \tag{20}$$

$$\frac{\Delta H^0_{\mathrm{WGS}}}{RT} = \sum_{j=1}^{N}\left(\nu''_j - \nu^j_j\right)\frac{h^0_j}{R} \tag{21}$$

where S^0_i and h^0_i are the standard-state entropy and standard-state enthalpy, respectively.

2.5. Electrochemical reactions

The hydrogen generated via the DISR and WGS reactions described above then undergoes the electrochemical reaction within the PEN structure as follows:

$$\mathrm{Anode:}\quad H_2 + O^{2-} \rightarrow H_2O + 2e^- \tag{22}$$

$$\mathrm{Cathode:}\quad \frac{1}{2}O_2 + 2e^- \rightarrow O^{2-} \tag{23}$$

$$\mathrm{Net:}\quad H_2 + \frac{1}{2}O_2 \rightarrow H_2O \tag{24}$$

The electrochemical reaction is assumed to take place near the (TPB) triple-phase-boundary within the anode layer for the present anode-supported design. Basically, CO can also carry out the electrochemical reaction in a SOFC, but the reaction rate is much lower than that of H_2 oxidation [22,25]. Therefore, only the electrochemical reaction of H_2 is considered in the present model.

2.6. Electrochemical model

The cell voltage is related to the open circuit voltage and three polarization loss terms. The open circuit voltage is calculated by the Nernst equation:

$$E_{\mathrm{OCV}} = E_0 + \frac{RT}{nF}\ln\left(\frac{p^{\mathrm{tpb}}_{H_2}\,p^{\mathrm{tpb}^{1/2}}_{O_2}}{p^{\mathrm{tpb}}_{H_2O}}\right) \tag{25}$$

The open circuit voltage is affected by the partial pressure of related species in the triple phase boundary. The theoretical potential E_0 is given as

$$E_0 = \frac{-\Delta G^0}{nF} \tag{26}$$

where the ΔG^0 is the Gibb's free energy for the electrochemical reaction of hydrogen. The cell voltage is evaluated by:

$$V_{\mathrm{cell}} = E_{\mathrm{ocv}} - iR_{\mathrm{ohm}} - \eta_{\mathrm{act,a}} - \eta_{\mathrm{act,c}} - \eta_{\mathrm{conc}} \tag{27}$$

where $\eta_{\mathrm{act,a}}$ and $\eta_{\mathrm{act,c}}$ stand for the activation loss for the anode and the cathode, respectively. It can be described by the Butler–Volmer equation:

$$i_{\mathrm{cell}} = i_{0,\mathrm{electrode}}\left[\exp\left(\frac{\beta nF\eta_{\mathrm{act,electrode}}}{RT}\right) - \exp\left(\frac{(1-\beta)nF\eta_{\mathrm{act,electrode}}}{RT}\right)\right] \tag{28}$$

where the electrode includes the anode and the cathode. There were two approaches reported to estimate the activation polarization [26]. For the first approach, the expressions for activation polarizations of the two electrodes are different [27]. For the second approach, the transfer coefficient (β in Eq. (28)) is assumed as 0.5 [13,22,28–32]. Therefore, the Butler–Volmer equation (Eq. (28)) can be rewritten into an explicit form, and the same expression can be employed to both electrodes with the different exchange current densities. In the present study, the second approach is employed in the electrochemical model and the exchange current density in Eq. (28) is determined by [29]:

$$i_{0,\mathrm{anode}} = K_{\mathrm{anode}}\left(\frac{p^{\mathrm{TPB}}_{H_2}}{P}\right)\left(\frac{p^{\mathrm{TPB}}_{H_2O}}{P}\right)\exp\left(\frac{-E_{\mathrm{act,anode}}}{RT}\right) \tag{29}$$

$$i_{0,\mathrm{cathode}} = K_{\mathrm{cathode}}\left(\frac{p^{\mathrm{TPB}}_{O_2}}{P}\right)^{0.25}\exp\left(\frac{-E_{\mathrm{act,cathode}}}{RT}\right) \tag{30}$$

where the pre-exponential factor (K) is 5.5×10^8 A m^{-2} for the anode and 7×10^8 A m^{-2} for the cathode [29]. The activation energy (E_{act}) is 100×10^3 J mol^{-1} for the anode and 120×10^3 J mol^{-1} for the cathode [29]. The concentration loss in Eq. (27) is due to mass diffusion for the reactants and products within the electrode, and can be described by [29]:

$$\eta_{conc} = -\frac{RT}{nF}\ln\left(\frac{p_{H_2}p^{ref}_{H_2O}}{p^{ref}_{H_2}p_{H_2O}}\right) \quad (31)$$

.

Since the cell is anode-supported, the concentration loss on the cathode side is negligible [22]. The parameters for the activation loss are adopted from the study of Costamagna et al. [29,33]. The physical properties of the materials used in the present model are given in Table 2.

For the numerical method of the FV model, the scalars will be stored at the cell center, while face values are interpolated from the cell-center value using the upwind scheme. The upwind scheme interpolation is employed for the density, momentum, species and energy equations. The computational grid was tested to confirm the grid independency. The government equations are solved by the pressure-based solver [14]. Therefore, the momentum and continuity equations are solved simultaneously as step one. After updating the mass flux, the species and energy equations are solved as step two. If the convergence criterion is met, the iteration will be terminated. Otherwise the properties are updated and back to step one to initiate a new iteration loop until the convergence criterion is met.

2.7. Anode-recycling mechanism

The anode-recycling mechanism is employed in the start-up process by mixing the anode exhaust gas with fuel before the SOFC module [1]. It is expected to reduce the required start-up time and the corresponding temperature gradient. The extent of the anode-recycling is defined as:

$$Y_{i,\gamma\%} = Y_{i,out} \times \gamma\% + Y_{i,inlet} \times (1 - \gamma\%) \quad (32)$$

Under the anode-recycling condition, a specified amount, i.e., γ % in Eq. (32), of the inlet species is replaced by the outlet gas. The anode-recycling mechanism is first employed to the steady-state simulation and compared with the reference result as a validation. Next, it will be incorporated into the start-up process for the case using methane.

2.8. Fixed-temperature-difference mechanism

For the fixed-temperature-difference mechanism, the temperature difference to be fixed is defined as the difference between the inlet temperature and the minimum temperature of the PEN structure as:

$$T_{inlet} = T_{cell\_min} + \Delta T \quad (33)$$

This mechanism is employed to the case utilizing the hydrogen and methane to examine its performance on the start-up process.

2.9. Simulation approaches and procedures

In the present study, the results of the thermal behavior, the start-up time and the corresponding temperature gradient are investigated for an anode-supported planar SOFC during the start-up process. The validation of the proposed model is presented by comparing the polarization curve of the cell and the cell temperature profile with those of relevant studies. The hydrogen and methane are employed in the start-up process of the SOFC. First, the effect of different fuels on the start-up performance is investigated. Next, the anode-recycling mechanism is incorporated to verity its effect on the start-up process. Finally, the mechanism of the fixed-temperature-difference is employed to explore whether it is able to reduce the start-up time and the effective maximum absolute temperature-gradient (the largest one during the whole process). The start-up time and the effective maximum absolute temperature-gradient are taken as the criteria to evaluate the performance of the start-up mechanism.

3. Results and discussion

3.1. The validation of the finite-volume model

Numerical validation is made for the FV model. The calculated current–voltage curve is first compared with the experiment data [29], as shown in Fig. 2. The trends of the predicted and experiment results match with each other. The difference is about 3% within the range from 0.5 to 1.0 V, validating the electrochemical model. Next, the temperature profile, as shown in Fig. 3, is compared with that of Nikooyeh et al. [13] for the case of $V = 0.7$ V to validate the chemical reaction for methane feedstock. The inlet conditions, geometric parameters, and operating conditions are adopted from the compared reference [13]. Since the material properties were not reported in the paper of Nikooyeh et al. [13], typical material properties for the anode (Ni-YSZ), the electrolyte (YSZ) and the cathode (LSM) are assumed in the present study [31,34,35]. The interconnector uses stainless steel [34]. As shown in Fig. 3, the temperature profiles predicted in the present study are in good agreement with those by Nikooyeh et al. [13]. The overall temperature difference is less than 1%. Furthermore, the maximum temperature gradient (17 K cm^{-1}), shown in Fig. 3, also matches closely with the compared data (16 K cm^{-1}) [13], validating the present FV model.

3.2. Effect of different fuel on the start-up process

The effect of different fuels, i.e., hydrogen and methane, on the start-up process is investigated in this section. For the case using hydrogen, the variation of the average cell-temperature during the start-up process is shown in Fig. 4a, while the variation of the effective maximum absolute temperature-gradient for the first 10 s is shown in Fig. 4b. At the beginning of the start-up process, the average cell-temperature increases relatively fast (Fig. 4a), leading to the largest effective maximum absolute temperature-gradient (Fig. 4b). When the increasing cell-temperature is close to the

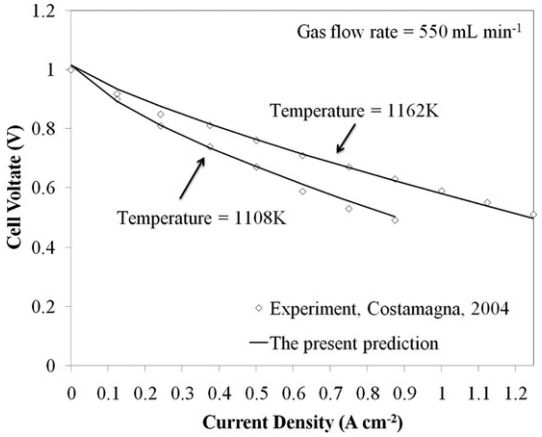

Fig. 2. Comparison of the predicted current–voltage curve with the experimental data [29].

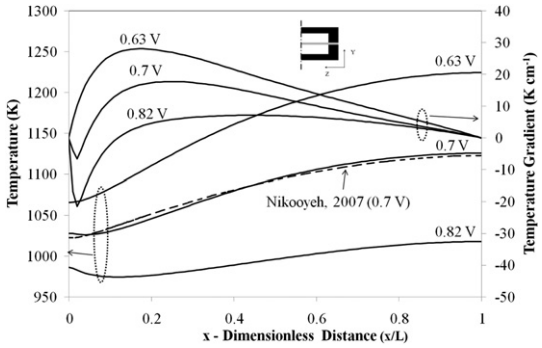

Fig. 3. Temperature profiles under various operating conditions and the corresponding temperature-gradient distributions in comparison with Nikooyeh et al. [13].

inlet temperature (1073 K), the start-up pace slows down and a smaller effective maximum absolute temperature-gradient is exhibited (Fig. 4b), since the difference between the cell temperature and the inlet temperature reduces. The whole start-up process takes about 14 min. The largest effective maximum absolute temperature-gradient is about 113.6 K cm^{-1}, which occurs at about 1.6 s from the beginning of the start-up process. The temporal variation of the cell-temperature distribution during the start-up process is shown in Fig. 5a, while the corresponding variation of the temperature-gradient distribution is shown in Fig. 5b. The initial temperature distribution (at 0 s) is adopted from the heat-up results of the counter-flow configuration in our previous study [5], where the largest maximum absolute temperature-gradient is

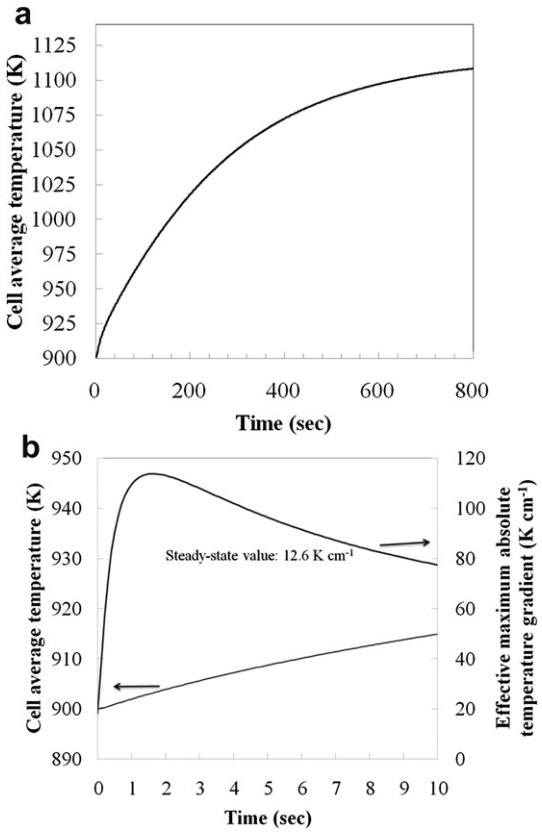

Fig. 4. (a) Temperature variation and (b) the corresponding variation of the effective maximum absolute temperature-gradient within the first 10 s for the case utilizing the hydrogen in the start-up process.

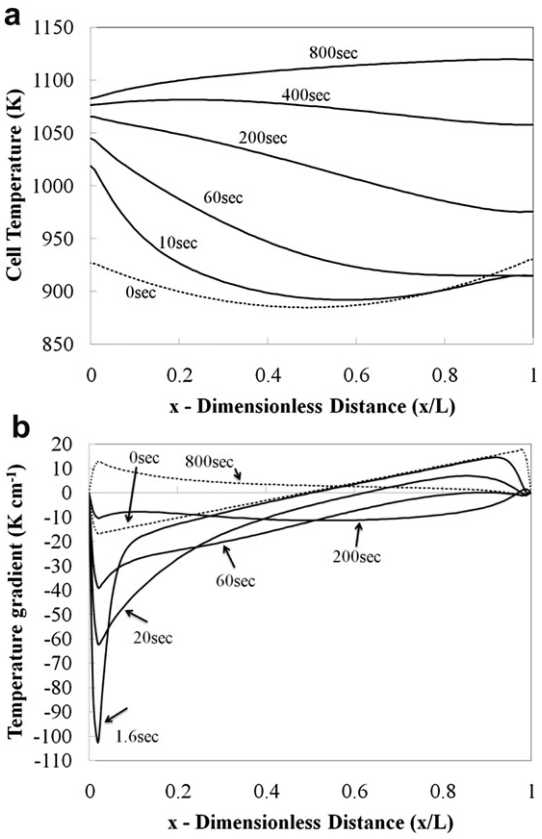

Fig. 5. (a) Variation of the temperature distribution and (b) the corresponding variation of the distribution of the temperature gradient for the case utilizing the hydrogen in the start-up process.

about 16 K cm^{-1} (Fig. 5b). As the high-temperature hydrogen is introduced from the fuel inlet, the temperature near the inlet increases drastically. Since the downstream temperature has not caught up with the pace of the inlet region, the largest effective maximum absolute temperature-gradient (113.6 K cm^{-1}) is exhibited near the inlet region at the beginning of the start-up process (Fig. 5b). After that, as the downstream temperature increases, the absolute temperature-gradient near the inlet region gradually decreases. At about 200 s from the beginning of the start-up process, the absolute temperature-gradient (15 K cm^{-1}) reduces to the level of the initial condition of the start-up process. At about 400 s from the beginning of the start-up process, the downstream temperature gradually becomes larger than that near the inlet region (Fig. 5a). At 800 s from the beginning of the start-up process, the temperature gradient turns to positive near the inlet region (Fig. 5b) as the downstream temperature becomes larger than that of the upstream region (Fig. 5a). It is noticeable that the feeding fuel heats the cell at the beginning of the start-up process, while it cools the cell at the later stage of the start-up process. This role-transformation was also observed in the study of Selimovic et al. [9] for the start-up process of a SOFC.

For the case using methane to start-up the SOFC, the variation of the average cell temperature during the start-up process is shown in Fig. 6a, while the variation of the effective maximum absolute temperature-gradient for the first 50 s is shown in Fig. 6b. The trend of the variation of the average cell-temperature is similar to that using hydrogen with a much slower pace. The whole process takes about 45 min, and the effective maximum absolute temperature-gradient is about 53 K cm^{-1}, occurring at about 9.5 s from the beginning of the start-up process. It is noticeable that the average

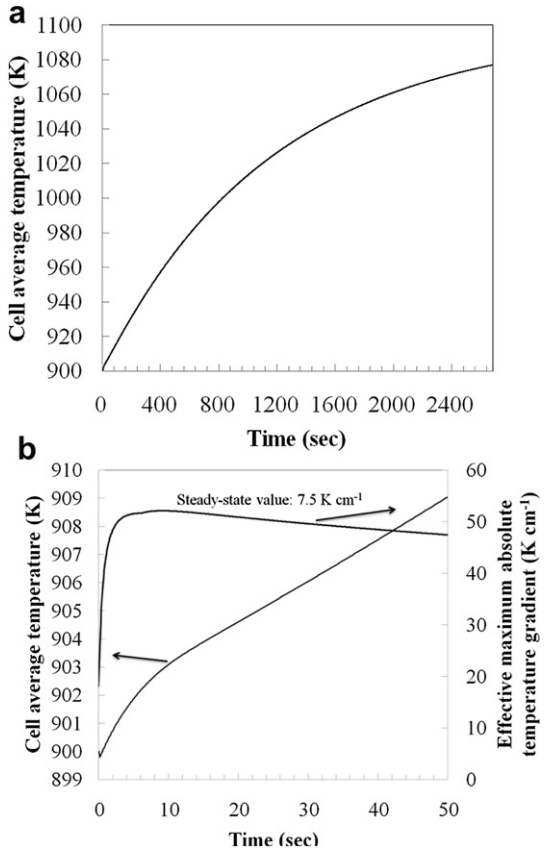

Fig. 6. Variation of the (a) temperature and (b) the corresponding temperature gradient for the case utilizing the methane in the start-up process.

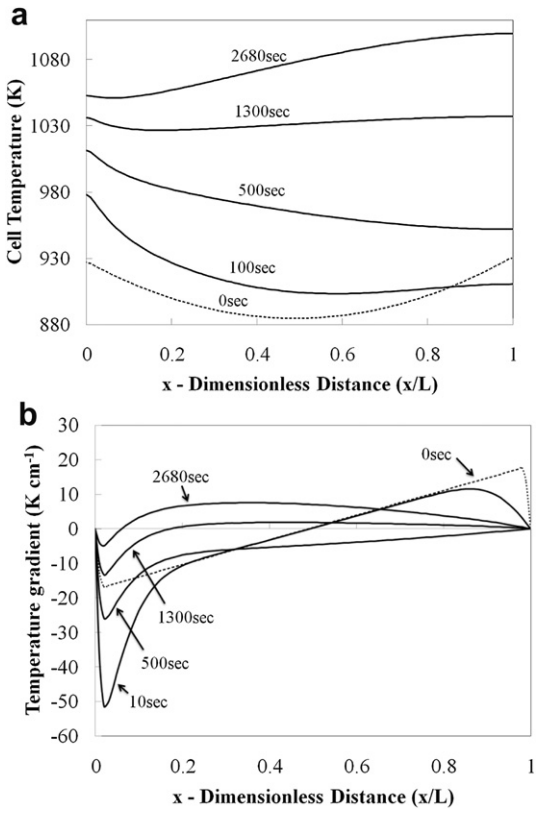

Fig. 7. (a) Variation of the temperature distribution and (b) the corresponding variation of the distribution of the temperature gradient for the case utilizing the methane in the start-up process.

cell temperature drops slightly at the beginning of the start-up process. This is because the hydrogen-required, exothermic electrochemical reaction takes place only after the endothermic internal reforming reaction has proceeded, leading to a small dip of the cell temperature at the beginning of the start-up process. The temporal variation of the cell-temperature distribution is shown in Fig. 7a, while the corresponding variation of the temperature-gradient distribution is shown in Fig. 7b. The temporal variation of the temperature distribution is similar to that of the case using hydrogen. In the early stage, the temperature near the inlet region increases, resulting in the largest effective maximum absolute temperature-gradient. However, the extent is much smaller than that of the case utilizing hydrogen. The temperature rising pace is slower for the case using methane, since the hydrogen for the exothermic electrochemical reaction is not directly provided, but generated via the internal reforming and the water-gas-shift reaction. Besides, the endothermic internal reforming reaction moderates some extent of the thermal energy provided by the gas fed at the inlet. The effective maximum absolute temperature-gradient for the case utilizing methane is reduced by 54%, compared to that utilizing hydrogen.

A comprehensive comparison for the effect of different fuels on the start-up performance is shown in Fig. 8. The time required for the start-up process for the case utilizing methane is about 45 min and 3.2 times longer than that using hydrogen. This is because the hydrogen for the electrochemical reaction has to be generated from the steam-reforming reaction for the case utilizing methane. For the APU system, however, a start-up process taking more than 40 min is too slow [8]. The effective maximum absolute temperature-gradient for the case using hydrogen is 2.2 times larger than that utilizing methane. This is because the endothermic internal reforming reaction of methane consumes some thermal energy from the feeding gas, narrowing down the temperature difference between the inlet and the interior in the early stage. At the end of the start-up process, the temperature gradients are comparable for both fuels. Therefore the effect of different fuels on the temperature uniformity of the SOFC system is more significant at the beginning of the start-up process. The commonly referred statement that the endothermic internal reforming reaction generates a large temperature-gradient [13,22,24,30,36] may be true in the steady-state operation, while it is a positive effect on the

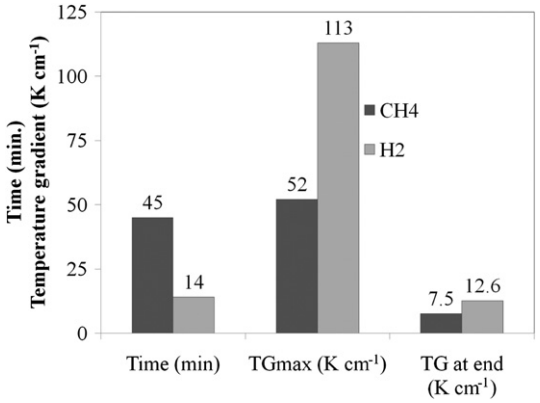

Fig. 8. Comprehensive comparison of the results by utilizing different fuel in the start-up process (*TGmax* is the effective maximum absolute temperature-gradient, and *TG at end* is the temperature-gradient at the end of the start-up process).

accommodation of the temperature uniformity during the start-up process. Therefore, the internal reforming reaction is favorable in the start-up process, since it moderates the large temperature gradient.

3.3. Effect of the anode-cycling on the start-up process

The temperature distributions at the steady state under the anode-recycling conditions are shown in Fig. 9a, while the temperature-gradient distributions are shown in Fig. 9b. The temperature near the inlet region increases with the increasing extent of the anode-recycling (Fig. 9a). This is because the mass fraction of the methane reduces, leading to a less extent of the endothermic internal reforming reaction. For the downstream region, the temperature increases with the increasing extent of the anode-recycling, since some hydrogen is introduced via the recycling, leading to a larger current density (0.57 A cm^{-2} without anode-recycling and 0.71 A cm^{-2} for 70% anode-recycling). For the temperature gradient, the maximum-temperature-gradient reduces with the increasing extent of the anode-recycling, and its position shifts toward the inlet region (Fig. 9b). As the extent of the anode-recycling increases to 70%, the negative temperature gradient near the inlet region vanishes. This is because the endothermic internal reforming reaction reduces with the reduction of the mass fraction of methane. As 70% of the anode-recycling mechanism is employed, the maximum-temperature-gradient reduces from 17 K cm^{-1} to 12 K cm^{-1} (decrease 5 K cm^{-1}), while it reduces from 16 K cm^{-1} to 10 K cm^{-1} (decrease 6 K cm^{-1}) in the study of Nikooyeh et al. [13]. Therefore, the effect of the anode-recycling mechanism at the steady state proposed by the present study is consistent with that in the literature [13].

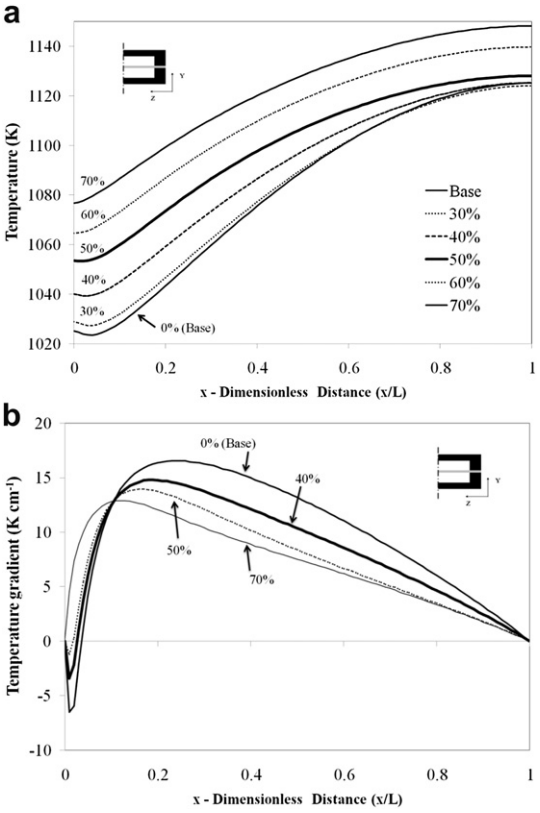

Fig. 9. (a) Temperature distributions and (b) temperature gradient distributions under the anode-recycling condition.

The anode-recycling mechanism is then incorporated into the start-up process, and the results about the start-up time and the effective maximum absolute temperature-gradient are shown in Fig. 10. The effect of the anode-recycling on the start-up time is significant. Compared to the base case (without anode-recycling), the start-up time is shortened by 29.29% for the 30% recycling, 40.75% for the 50% recycling, and 48.58% for the 70% recycling. This is because less methane and more hydrogen are introduced under the anode-recycling condition. Therefore, with the anode-recycling mechanism, less methane undergoes the complicated reactions of IR, WGS and EC (Electrochemical), while more hydrogen is directly converted to the electric power, leading to a faster start-up. However, the effect of the anode-recycling mechanism on the effective maximum absolute temperature-gradient is insignificant (<0.7%) in the start-up process. Therefore, the incorporation of the anode-recycling mechanism reduces the temperature gradient at the steady state, while it shortens the time required for the start-up process.

3.4. The fixed-temperature-difference start-up technique

As shown in the previous section, the high temperature-gradient, which occurs at the beginning of the start-up process, is due to the sudden increase of the inlet temperature to the operation value. An alternative start-up procedure is introduced in the present section, i.e., the fixed-temperature-difference mode. This method is expected to reduce the large temperature gradient at the beginning of the start-up process, and speed up the pace at the later stage. For the case using hydrogen, the temporal variation of the average cell-temperature and the effective maximum absolute temperature-gradient under different fixed temperature differences are shown in Fig. 11. It is found that for the case of a fixed 100 K temperature-difference, the temperature rising rate is slower than that of the original case, while the effective maximum absolute temperature-gradient is 49.3 K cm^{-1} which is also smaller than that of the original case. For the case of a fixed 175 K temperature-difference, the effective maximum absolute temperature-gradient is comparable with that of the original case. The effective maximum absolute temperature-gradient for the case of a fixed 250 K temperature-difference is, however, larger than that of the original case. A comprehensive comparison of the effective maximum absolute temperature-gradient and the start-up time is

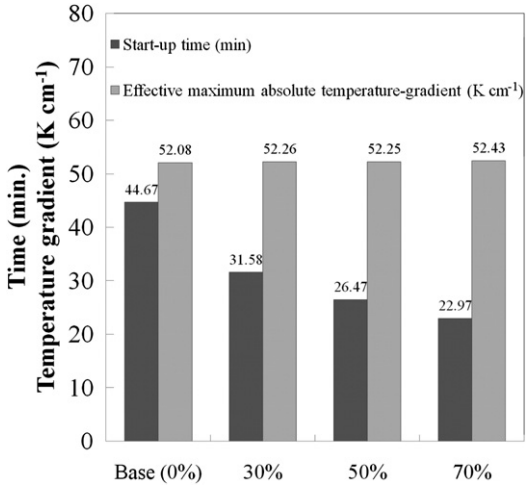

Fig. 10. Effect of the anode-recycling mechanism on the start-up time and the effective maximum absolute temperature-gradient.

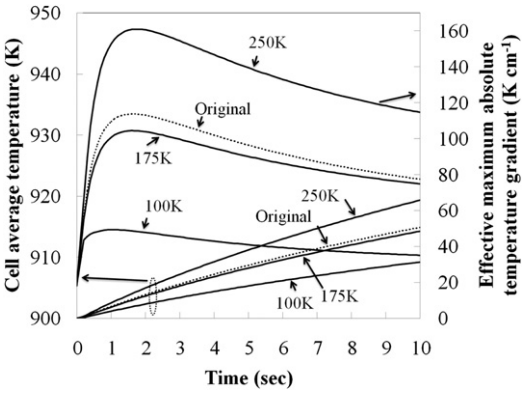

Fig. 11. Temperature variation and the corresponding variation of the effective maximum absolute temperature-gradient within the first 10 s for the case utilizing the hydrogen and the fixed temperature difference mode in the start-up process.

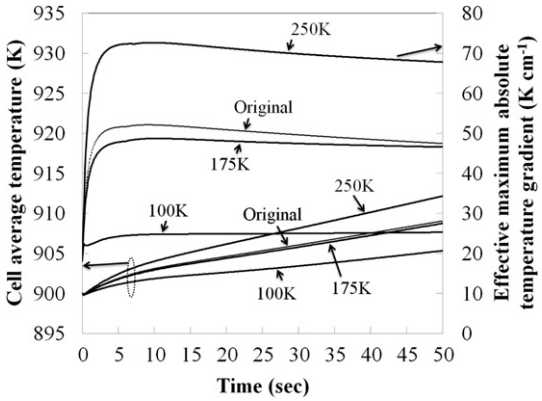

Fig. 13. Temperature variation and the corresponding variation of the effective maximum absolute temperature-gradient within the first 50 s for the case utilizing the methane and the fixed temperature difference mode in the start-up process.

shown in Fig. 12. Comparing the case of a fixed 100 K temperature-difference with the original one, it is noticeable that the time required for the start-up process is comparable, while the effective maximum absolute temperature-gradient is reduced by 56%. For the case of a fixed 175 K temperature-difference, the effective maximum absolute temperature-gradient is comparable with that of the original case, while the start-up time is shortened by 42%. For the case of a fixed 250 K temperature-difference, the effective maximum absolute temperature-gradient is 41% larger than that of original case, while the time required for the start-up is 58% shorter than that of the original case. Therefore, a properly selected temperature-difference of the inlet fuel and the cell may lead to a faster start-up pace and a smaller temperature gradient.

The results for the case using methane as the fuel under the mechanism of a fixed temperature-difference are shown in Fig. 13. It is found that for the case of a fixed 100 K temperature-difference, the temperature rising rate within the first 50 s is much slower than that of the original case, while the effective maximum absolute temperature-gradient is about 25 K cm^{-1} smaller than that of the original case. For the case of a fixed 175 K temperature-difference, the effective maximum absolute temperature-gradient is comparable with that of the original case. The effective maximum absolute temperature-gradient for the case of a fixed 250 K temperature-difference is, however, larger than that of the original case. A comprehensive comparison of the effective maximum absolute temperature-gradient and the start-up time is shown in Fig. 14. For the case of a fixed 100 K temperature-difference, the time required for the start-up process is about 37% and the effective maximum absolute temperature-gradient about 52% less than those of the original case. For the case of a fixed 175 K temperature-difference, the effective maximum absolute temperature-gradient is comparable, while the start-up time is reduced by 57%. For the case of a fixed 250 K temperature-difference, the effective maximum absolute temperature-gradient is 39% larger than that of the original case, while the start-up time is reduced by 67%. Therefore, for the case using methane, it is interesting to note that the start-up procedure of a fixed 100 K temperature-difference may reduce both the start-up time and the effective maximum absolute temperature-gradient. The reduction of the effective maximum absolute temperature-gradient is due to a relatively smaller inlet temperature, which is the main factor causing the increase of the absolute temperature-gradient at the beginning of the start-up process. At the later stage of the start-up process, the fixed-temperature-difference mechanism accelerates the start-up process and shortens the required time. In contrary, for the original start-up procedure, the temperature difference reduces substantially as the cell temperature approaches the inlet temperature, slowing down the start-up process. Therefore, for the start-up procedure using a fixed-temperature-difference mode, an optimal value for the temperature difference could be selected to speed up the start-up process, while keeping the effective maximum absolute temperature-gradient under the allowable threshold.

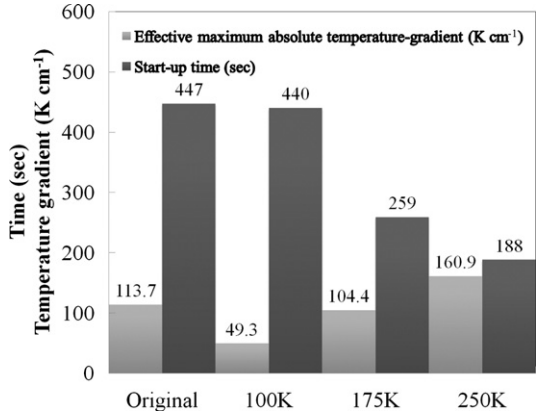

Fig. 12. Comprehensive comparison of the start-up time and the effective maximum absolute temperature-gradient for the case using hydrogen for the effect of the fixed temperature difference mechanism.

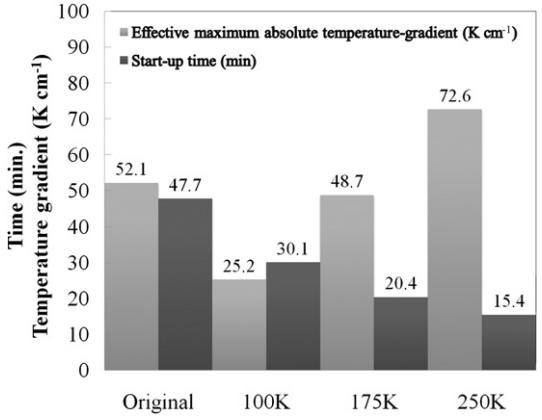

Fig. 14. Comprehensive comparison of the start-up time and the effective maximum absolute temperature-gradient for the case using methane for the effect of the fixed temperature difference mechanism.

4. Conclusions

For the start-up process of a SOFC system, both methane and hydrogen utilized as the fuel, respectively, have been investigated for their effects on the start-up process. The anode-recycling mechanism is tested at the steady state as a validation, and then incorporated into the start-up process to examine its performance. Finally, the performance of the fixed-temperature-difference mechanism is evaluated for the start-up process. Some conclusions are drawn from the present study as follows:

(1) For the start-up process using hydrogen as the fuel, the gas introduced at the inlet warms up the cell at the beginning of the start-up process, and turns to cool the cell at the later stage of the start-up process when the temperature of the cell is higher than that of the inlet gas. For the start-up process using methane as the fuel, there is a slightly temperature dip at the beginning of the start-up process due to the proceeding of the internal reforming reaction. The effective maximum absolute temperature-gradient is generated at the beginning of the start-up process for both cases. For the present investigated SOFC configuration, the start-up time for the case utilizing methane is 3.2 times longer than that using hydrogen. The effective maximum absolute temperature-gradient for the case using hydrogen is 2.2-fold larger than that utilizing methane. The endothermic internal reforming reaction of methane has a positive effect on the accommodation of the temperature uniformity during the start-up process.
(2) The effect of the anode-recycling on the start-up time is significant. Comparing to the base case, i.e., without anode-recycling, the start-up time is shortened by 29.29% for the 30% recycling, 40.75% for the 50% recycling, and 48.58% for the 70% anode-recycling for the present investigated SOFC configuration. However, the effect of the anode-recycling mechanism on the effective maximum absolute temperature-gradient is not significant.
(3) For the fixed-temperature-difference mechanism in the start-up process, a properly selected temperature-difference may lead to a shorter start-up time and a smaller effective maximum absolute temperature-gradient. The reduction of the effective maximum absolute temperature-gradient is due to a smaller inlet temperature in the early stage of the start-up process. In the later stage of start-up process, the fixed temperature-difference accelerates the process and shortens the required time. Therefore, the start-up process can be accelerated by choosing an optimal value for the temperature difference, while keeping the effective maximum absolute temperature-gradient under an allowable threshold.

Acknowledgement

This work was sponsored by the National Science Council of Taiwan under contract No. NSC 98-2221-E-006-231.

References

[1] T. Kivisaari, P. Bjornbom, C. Sylwan, B. Jacquinot, D. Jansen, A. De Groot, Chemical Engineering Journal 100 (2004) 167–180.
[2] S.C. Singhal, Solid State Ionics 152–153 (2002) 405–410.
[3] C. Stiller, B. Thorud, S. Seljeb, O. Mathisen, H. Karoliussen, O. Bolland, Journal of Power Sources 141 (2005) 227–240.
[4] T.L. Jiang, M.H. Chen, International Journal of Hydrogen Energy 34 (2009) 8223–8234.
[5] M.H. Chen, T.L. Jiang, International Journal of Hydrogen Energy 36 (2011) 6882–6893.
[6] Y.M. Barzi, M. Ghassemi, M.H. Hamedi, International Journal of Hydrogen Energy 34 (2008) 2015–2025.
[7] P.K. Cheekatamarla, C.M. Finnerty, J. Cai, International Journal of Hydrogen Energy 33 (2008) 1853–1858.
[8] L. Petruzzi, S. Cocchi, F. Fineschi, Journal of Power Sources 118 (2003) 96–107.
[9] A. Selimovic, M. Kemm, T. Torisson, M. Assadi, Journal of Power Sources 145 (2005) 463–469.
[10] Z. Wang, J.O. Berghaus, S. Yick, C. Deces-Petit, W. Qu, R. Hui, R. Maric, D. Ghosh, Journal of Power Sources 176 (2008) 90–95.
[11] P.H. Lin, C.W. Hong, Journal of Power Sources 160 (2006) 1230–1241.
[12] P.H. Lin, C.W. Hong, Journal of Power Sources 187 (2009) 517–526.
[13] K. Nikooyeh, A.A. Jeje, J.M. Hill, Journal of Power Sources 171 (2007) 601–609.
[14] Fluent 6.3, User Guide, Fluent Incorporated, 2006.
[15] J. Van Herle, D. Larrain, N. Autissier, Z. Wuillemin, M. Molinelli, D. Favrat, Journal of the European Ceramic Society 25 (2005) 2627–2632.
[16] J. Ki, D. Kim, Journal of Power Sources 195 (2010) 3186–3200.
[17] T. Tanaka, Y. Inui, A. Urata, T. Kanno, Energy Conversion and Management 48 (2007) 1491–1498.
[18] X. Xue, J. Tang, N. Sammes, Y. Du, Journal of Power Sources 142 (2005) 211–222.
[19] Y. Ji, K. Yuan, J.N. Chung, Y.-C. Chen, Journal of Power Sources 161 (2006) 380–391.
[20] Y. Qi, B. Huang, J. Luo, Chemical Engineering Science 61 (2006) 6057–6076.
[21] A. Musa, M. De Paepe, International Journal of Hydrogen Energy 33 (2008) 4665–4672.
[22] P. Aguiar, C.S. Adjiman, N.P. Brandon, Journal of Power Sources 138 (2004) 120–136.
[23] E. Achenbach, Journal of Power Sources 49 (1994) 333–348.
[24] B.A. Haberman, J.B. Young, International Journal of Heat and Mass Transfer 47 (2004) 3617–3629.
[25] M.A. Khaleel, Z. Lin, P. Singh, W. Surdoval, D. Collin, Journal of Power Sources 130 (2004) 136–148.
[26] Y.P. Chyou, J.S. Chen, T.D. Chung, Journal of the Electrochemical Society 155 (2008) B650–B659.
[27] M. Iwata, T. Hikosaka, M. Morita, T. Iwanari, K. Ito, K. Onda, Y. Esaki, Y. Sakaki, S. Nagata, Solid State Ionics 132 (2000) 297–308.
[28] S.H. Chan, K.A. Khor, Z.T. Xia, Journal of Power Sources 93 (2001) 130–140.
[29] P. Costamagna, A. Selimovic, M. Del Borghi, G. Agnew, Chemical Engineering Journal 102 (2004) 61–69.
[30] P. Aguiar, C.S. Adjiman, N.P. Brandon, Journal of Power Sources 147 (2005) 136–147.
[31] J.J. Hwang, C.K. Chen, D.Y. Lai, Journal of Power Sources 140 (2005) 235–242.
[32] L.K. Chiang, H.C. Liu, Y.H. Shiu, C.H. Lee, R.Y. Lee, Renewable Energy 33 (2008) 2580–2588.
[33] P. Costamagna, K. Honegger, Journal of the Electrochemical Society 145 (1998) 3995–4007.
[34] D.L. Damm, A.G. Fedorov, Journal of Power Sources 159 (2006) 956–967.
[35] H.Y. Jung, W.S. Kim, S.H. Choi, H.C. Kim, J. Kim, H.W. Lee, J.H. Lee, Journal of Power Sources 155 (2006) 145–151.
[36] H. Yakabe, T. Ogiwara, M. Hishinuma, I. Yasuda, Journal of Power Sources 102 (2001) 144–154.